Brownian Dynamics Simulations of the Recognition of the Scorpion Toxin Maurotoxin with the Voltage-Gated Potassium Ion Channels

Wei Fu,* Meng Cui,† James M. Briggs,† Xiaoqin Huang,* Bing Xiong,* Yingmin Zhang,* Xiaomin Luo,* Jianhua Shen,* Ruyun Ji,* Hualiang Jiang,* and Kaixian Chen*

*Center for Drug Discovery and Design, State Key Laboratory of Drug Research, Shanghai Institute of Meteria Medica, Shanghai Institutes of Biological Sciences, Chinese Academy of Sciences, Shanghai 200031, China; †Department of Biology and Biochemistry, University of Houston, Houston, Texas 77204 USA

ABSTRACT The recognition of the scorpion toxin maurotoxin (MTX) by the voltage-gated potassium (Kv1) channels, Kv1.1, Kv1.2, and Kv1.3, has been studied by means of Brownian dynamics (BD) simulations. All of the 35 available structures of MTX in the Protein Data Bank (http://www.rcsb.org/pdb) determined by nuclear magnetic resonance were considered during the simulations, which indicated that the conformation of MTX significantly affected both the recognition and the binding between MTX and the Kv1 channels. Comparing the top five highest-frequency structures of MTX binding to the Kv1 channels, we found that the Kv1.2 channel, with the highest docking frequencies and the lowest electrostatic interaction energies, was the most favorable for MTX binding, whereas Kv1.1 was intermediate, and Kv1.3 was the least favorable one. Among the 35 structures of MTX, the 10th structure docked into the binding site of the Kv1.2 channel with the highest probability and the most favorable electrostatic interactions. From the MTX-Kv1.2 binding model, we identified the critical residues for the recognition of these two proteins through triplet contact analyses. MTX locates around the extracellular mouth of the Kv1 channels, making contacts with its β-sheets. Lys23, a conserved amino acid in the scorpion toxins, protrudes into the pore of the Kv1.2 channel and forms two hydrogen bonds with the conserved residues Gly401(D) and Tyr400(C) and one hydrophobic contact with Gly401(C) of the Kv1.2 channel. The critical triplet contacts for recognition between MTX and the Kv1.2 channel are Lys23(MTX)-Asp402(C)(Kv1), Lys27(MTX)-Asp378(D)(Kv1), and Lys30(MTX)-Asp402(A)(Kv1). In addition, six hydrogen-bonding interactions are formed between residues Lys23, Lys27, Lys30, and Tyr32 of MTX and residues Gly401, Tyr400, Asp402, Asp378, and Thr406 of Kv1.2. Many of them are formed by side chains of residues of MTX and backbone atoms of the Kv1.2 channel. Five hydrophobic contacts exist between residues Pro20, Lys23, Lys30 and Tyr32 of MTX and residues Asp402, Val404, Gly401, and Arg377 of the Kv1.2 channel. The simulation results are in agreement with the previous molecular biology experiments and explain the binding phenomena between MTX and Kv1 channels at the molecular level. The consistency between the results of the BD simulations and the experimental data indicated that our three-dimensional model of the MTX-Kv1.2 channel complex is reasonable and can be used in additional biological studies, such as rational design of novel therapeutic agents blocking the voltage-gated channels and in mutagenesis studies in both the toxins and the Kv1 channels. In particular, both the BD simulations and the molecular mechanics refinements indicate that residue Asp378 of the Kv1.2 channel is critical for its recognition and binding functionality toward MTX. This phenomenon has not been appreciated in the previous mutagenesis experiments, indicating this might be a new clue for additional functional study of Kv1 channels.

INTRODUCTION

During the last decade, interest has increased tremendously in the rational design of drugs acting on potassium channels (Hoshi et al., 1990; Goldstein et al., 1994; Legros et al., 2000; Carlier et al., 2001). Several excellent reviews (Chandy and Gutman, 1995; Goldstein and Colatsky, 1996; Kaczorowski et al., 1999) have dealt with the structural features that underlie particular biophysical and pharmacological properties of potassium channels. Recent research (Kaczorowski et al., 1999) has focused on the Kv1 channels and indicated that Kv1 family members may also constitute novel therapeutic targets. Voltage-gated (Kv1) potassium channels are widely distributed in the central and peripheral nervous system. Lacking this channel will result in some diseases such as spontaneous epileptic seizures (Smart et al., 1998), learning deficiencies (Meiri et al., 1997), and pathophysiology of episodic ataxia/myokymia and neurotransmitter release (Brandt and Strupp, 1997). Therefore, it is very important to study the drugs that act on these Kv1 channel proteins. At present, a variety of experimental strategies have defined functional domains within these Kv1 channel proteins (Aiyar et al., 1995), and some thermodynamic mutant cycle analyses have been used to identify specific amino acid residues in the S5-S6 linker region that are part of the scorpion-toxin receptor site (Aiyar et al., 1995; Doyle et al., 1998; Mackinnon et al., 1998). However, many questions are still unresolved because of experimental difficulties and the lack of significant theoretical guidance. All drugs now marketed that act on ion channels were discovered empirically rather than by molecular insight, and most have been shown to have serious safety and efficacy problems (Goldstein and Colatsky, 1996; Kaczorowski and Garcia, 1999). Therefore, theoretical simulations at the molec-

Submitted February 2, 2002, and accepted for publication June 28, 2002.

Address reprint requests to Dr. Hualiang Jiang and Jianhua Shen, Shanghai Institute of Meteria Medica, Chinese Academy of Sciences, 294 Taiyuan Road, Shanghai 200031, P. R. China. Tel.: 86-21-64318401; Fax: 86-21-64370269, E-mail: jiang@iris3.simm.ac.cn or jhshen@mail.shcnc.ac.cn

0006-3495/02/11/2370/16 $2.00

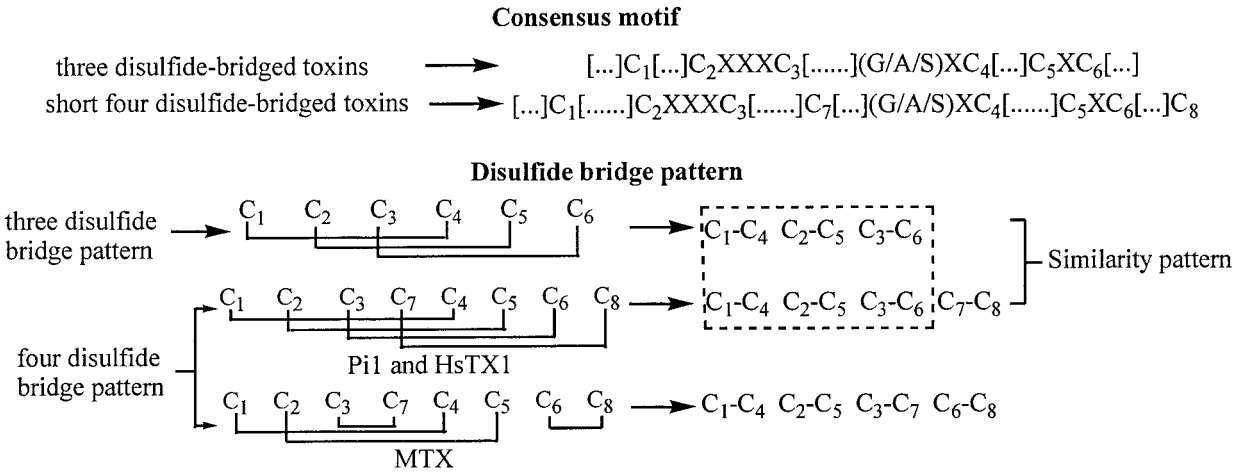

FIGURE 1 Consensus motif and disulfide bridge pattern of scorpion toxin.

ular level can be a powerful tool and will help to understand electrophysiological experiments performed on wild-type and mutant channels. Our interest in the mechanism of blockage of Kv1 channels stems from our efforts to design new ion channel blockers, with the eventual aim to develop new drugs for the treatment of diseases affecting both electrically excitable and nonexcitable tissues. In particular, our research is focused on the application of molecular simulation and modeling methods in the rational design of new blocking agents of Kv1 channels.

Scorpion toxins constitute the largest group of potassium channel blockers and are useful pharmacological probes to investigate ion-specific channel proteins and their functions (Kaczorowski and Garcia., 1999).

Maurotoxin (MTX; α-KTx6.2) is a unique toxin isolated from the venom of the Tunisian chactidae scorpion *Scorpio maurus palmatus* (Kharrat et al., 1997; Blanc et al., 1997). Compared with conventional three-disulfide-bridged scorpion toxins and two other recently reported toxins, Pi1 (Olamendi-Portugal et al., 1996) and HsTx1(Lebrun et al., 1997) from the venoms of the scorpions *Pandinus imperator* and *Heterometrus spinnifer*, respectively, MTX adopts an unusual disulfide bridge motif: the α-helix is connected by two disulfide bridges to two different strands of the β-sheet instead of connecting the α-helix to the same strand (Fig. 1). This uncommon toxin displays an exceptionally wide range of pharmacological activity, as it was found to show activity in the nanomolar range on both voltage-gated K^+ channels (Kv1.1, Kv1.2, Kv1.3, and *Shaker* B) and apamin-sensitive small-conductance Ca^{2+}-activated K^+ channels (SK) (Kharrat et al., 1996). The structural and pharmacological features of MTX (less than 40 residues, four disulfide bridges, and binding onto K^+ channels) suggest that MTX belongs to a new class of natural K^+ channel blockers structurally intermediate between the Na^+ (60–70 residues and four disulfide bridges) and K^+ channel scorpion toxin families (less than 40 residues and three disulfide bridges) (Darbon. et al., 1999). Recently, much attention has been paid to the pharmacological activity of MTX on the Kv1 channels (Fajloun et al., 2000a,b; Avdonin et al., 2000; Carlier et al., 2000, 2001). Like most scorpion toxins, MTX blocks the Kv1 channels by binding in the external vestibule of the pore to block the ion conduction pathway. Although Kv1.1, Kv1.2, and Kv1.3 have a very similar pore structure, they display different pharmacological activity inhibited by MTX, IC_{50} values are 37, 0.8, and 150 nM, respectively (Blanc et al., 1997). Particularly, it is worth noticing that MTX was described as a potent blocker of Kv1.2 (IC_{50} of 0.8 nM) compared with other known three-disulfide-bridged blockers such as noxiustoxin (IC_{50} of 2 nM) and charybdotoxin (IC_{50} of 14 nM) (Grissmer et al., 1994). Thus, MTX can be used as a structural probe to identify the critical residues of the nonconserved pore-forming sequence in the recognition of the Kv1 channels. Therefore, an understanding of the molecular interactions between MTX and the Kv1 channels, especially with the Kv1.2 channel, will provide insights into not only the conservation of the architecture of the Kv1 pores but also the mechanisms underlying the specificity of channel-toxin interaction.

However, no experimental data for the structure of MTX-Kv1 family channel complexes have been reported. In this study, by means of the Brownian dynamics (BD) method (Ermak and McCammon, 1978), the association of MTX (all of the 35 available structures in the Protein Data Bank; 1TXM) with Kv1.1, Kv1.2, and Kv1.3 was simulated. We first constructed the three-dimensional (3-D) structures of Kv1.1, Kv1.2, and Kv1.3 via homology modeling, taking the x-ray crystal structure of the KcsA K^+ channel as the model. We used the docking feature of BD simulations (Pearson and Gross, 1998; Ouporov et al., 1999) and the structural refinement functionality of molecular mechanics to identify the amino acid residues involved in complex formation, localize the regions of binding, estimate the

```
KcsA   ALHWRAAGAATVLLVIVLLAGSYLAVLAERGAPGAQLITYPRALWWSVETATTVGYGDLYPVTLWGRCVAVVVMVAGITSFGLVTAALATWFVGREQ
Kv1.2  KASMRELGLLIFFLFIGVILFSSAVYFAEADERDSQFPSIPDAFWWAVVSMTTVGYGDMVPTTIGGKIVGSLCAIAGVLTIALPVPVIVSNFNYFYH
            *  *    .:*.* ::  *  .  :** .  .:*: : * *:**:* : *******: *.*: *: *. :  :**: ::.* ...:.: *    :
```

FIGURE 2 Sequence alignments of KcsA (1BL8) with Kv1.2 channel generated by ClustalW. In the sequences, an asterisk indicates an identical or conserved residue, a colon indicates a conserved substitution, and a period indicates a semiconserved substitution (sequence identity is 28.9%; similarity is 62.9%).

strength of binding between the scorpion toxin MTX and the Kv1 family channels, and explain the affinity difference of MTX for the Kv1.1, Kv1.2, and Kv1.3 channel proteins.

MATERIALS AND METHODS

Atomic coordinates

The atomic coordinates of the scorpion toxin MTX (Blanc et al., 1997) and the K^+ channel KcsA (Doyle et al., 1998) were obtained from the Protein Data Bank at the Brookhaven National Laboratory (Bernstein et al., 1977), entries 1TXM and 1BL8, respectively.

Despite the unusual disulfide bridge pattern, MTX still adopts the conventional α/β scaffold; its conformation is grossly similar to those of other scorpion toxins. MTX contains a bent α-helix from residues 6–16 connected by two disulfide bridges (Cys9–Cys29 and Cys13–Cys19) to two different strands of the β-sheet (residues 23–26 and 28–31). Entry 1TXM contains 35 conformations of scorpion toxin MTX, which were obtained from nuclear magnetic resonance (NMR) spectroscopy; all of these structures were used in the BD simulations.

KcsA is the first and unique molecular description of an ion-selective channel. A remarkable structural conservation between the pore structures of a prokaryotic K^+ channel from *Streptomyces lividans* (KcsA) and the eukaryotic structure of voltage-dependent K^+ channels has recently been demonstrated by x-ray analysis (Mackinnon et al., 1998). Mackinnon et al. indicated that although KcsA subunits contain only two transmembrane segments, its amino acid sequence (in particular, its sequence in the pore region) is actually closer to those of eukaryotic six-membrane-spanning K^+ channels, and its pore structure and extracellular entryway are very similar to those of eukaryotic voltage-gated K^+ channels such as the *Shaker* K^+ channel from *Drosophila* and the vertebrate voltage-gated K^+ channels, which are believed to share essentially the same pore structure. Therefore, the 3-D structure of the KcsA K^+ channel, a protein isolated from the bacterium *S. lividans*, which was the first determined by x-ray crystallography at 3.2-Å resolution (Doyle et al., 1998), may be used as a template for modeling the 3-D structures of Kv channels. The 3-D structural models of Kv1.1, Kv1.2, and Kv1.3 channels were generated with the Homology module of Insight II (Molecular Simulation, San Diego, CA) based on the corrected KcsA structure, as described below.

Residues Arg27, Ile60, Arg64, Glu71, and Arg117, missing in the current KcsA x-ray structure, were added with the Biopolymer module of SYBYL Release 6.7 (Tripos, St. Louis, MO). The sequence alignment of KcsA (1BL8) with the Kv1.2 channel was generated by ClustalW (Thompson et al., 1994), which shows that the sequence identity between Kv1.2 and KcsA is 28.9%, and the similarity is 62.9%, as shown in Fig. 2. The protein backbone of the Kv1.2 homology model was identical to the KcsA backbone. The modeled side chains of the Kv1.2 channel were subjected to energy refinement (the gradient tolerance was achieved to 0.05 kcal mol^{-1} $Å^{-1}$, and a distance-dependent dielectric constant of 4 was used to simulate the effect of solvent), using the adopted-basis Newton Raphson algorithm and the CHARMM22 force field as implemented in the Quanta program (Quanta Release 98, Molecular Simulation) to relieve possible steric clashes and overlaps. With the same method as for the Kv1.2 channel, the 3-D structural models of the Kv1.1 and Kv1.3 channels were generated.

In a more sophisticated treatment, the membrane around the channel should be considered during the simulation. However, the mutagenesis and simulations (Aiyar et al., 1995) indicated that the scorpion toxins bind with the extracellular part of the potassium ion channel, where the electrostatics might not be affected by the membrane, for the membrane interacts only with the transmembrane parts of the channel. Therefore, we did not add the membrane into the simulation for computational facility.

BD simulation

The program package MacroDox version 3.2.2 (Northrup et al., 1999) was used to assign the titratable charges on proteins, solve the linearized Poisson-Boltzmann equation, and run the various BD simulations for the association between the scorpion toxin MTX and the Kv1 channels. The MacroDox program uses a test charge approach in BD simulation and is suitable for studying toxin-channel interaction and their mutual recognition (see Appendix). The BD algorithm for this program has been detailed by Northrup et al. (1987, 1993). The new updated charge file of CHARMM22 was used to assign the charges of the Kv1.1, Kv1.2, and Kv1.3 channels as well as MTX. The surface-accessibility-modified Tanford-Kirkwood calculations were performed using the method of Matthew (Matthew, 1985; Matthew and Gurd, 1986) to determine the protonation status of each titratable residue in the two proteins at pH 7.0 and ionic strength 0.1 M. MTX has four disulfide bonds, so the charges of the sulfur atoms of residues Cys3, Cys9, Cys13, Cys19, Cys24, Cys29, Cys31, and Cys34 were zeroed out. The Tanford-Kirkwood recommended partial charges were assigned to the Kv1 channels, and formal charges were assigned to MTX. The total charges are -13.16 e, -11.03 e, and -8.24 e for the Kv1.1, Kv1.2, and Kv1.3 channel, respectively, and 5.85 e for each of the 35 structures of MTX.

Following charge assignments, the electrostatic potentials about the Kv1 channels and MTX were determined by numerically solving the linearized Poisson-Boltzmann equation:

$$-\nabla\varepsilon\nabla\phi + \varepsilon\kappa^2\phi = \rho, \qquad (1)$$

where ϵ is the dielectric constant, κ is the inverse Debye length, ϕ is the electrostatic potential, and ρ is the charge density. Taking the above assigned charges as initial values, Eq. 1 was solved by the Warwicker-Watson method (Warwicker and Watson, 1982) as implemented in the MacroDox program (Northrup et al., 1999). The electrostatic potentials were determined on $61 \times 61 \times 61$ cubic grids centered on the center of mass of the two proteins. The protein interior dielectric constant and solvent dielectric constants were set as 4.0 and 78.3, respectively. The resolutions of inner grid and outer grid for the Kv1.1, Kv1.2, and Kv1.3 channels were chosen from the default values in the MacroDox program, 1.3 and 3.9 Å, respectively. Electrostatic focusing was used such that a low-resolution grid (3.9-Å spacing between grid points) was generated first and then used to obtain more accurate boundary potentials for a second, higher-resolution focused grid (1.3-Å spacing). The electrostatic potentials as shown in Fig. 3 were visualized by the GRASP program (Nicholls et al., 1991).

The BD simulations of the two interacting macromolecules in a continuum solvent dielectric was run stochastically through a series of small displacements chosen from a distribution that is equivalent to the short time

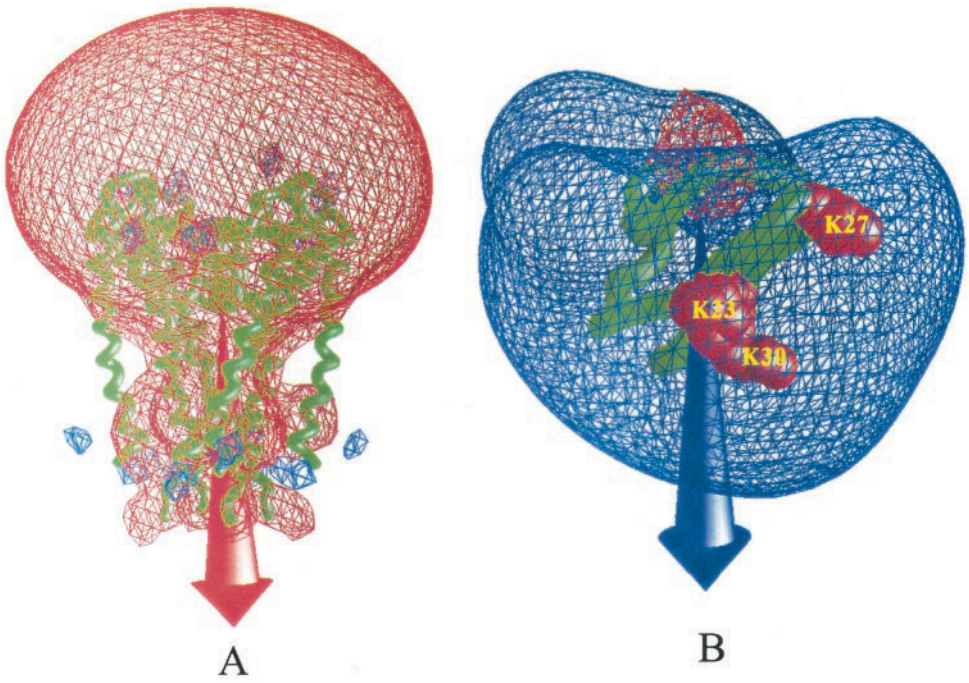

FIGURE 3 The electrostatic potential contour maps for the Kv1.2 channel and the scorpion toxin MTX. (*A*) Electrostatic potential for the Kv1.2 channel. The red contours represent isopotential surfaces where charge 1e possesses electrostatic potential energy equal to −2.5 kT; the blue isopotential surfaces are for energy +2.5 kT. (*B*) Electrostatic potential for the scorpion toxin MTX. The red contours represent isopotential surfaces where charge 1e possesses electrostatic potential energy equal to −2.5 kT; the blue isopotential surfaces are for energy +2.5 kT. Arrows indicate the directions of the dipoles in the proteins. The figure was generated with the program GRASP.

solution of the Smoluchowski diffusion equation (Smoluchowski, 1917) derived from several forces. The basic Ermak-McCammon algorithm (Ermak and McCammon, 1978) was used to simulate the translational Brownian motion of two interacting proteins as the displacements $\Delta\mathbf{r}$ of the relative separation vector $\mathbf{r}$ between the centroids of the two proteins in a time step Δt according to the relation:

$$\Delta\mathbf{r} = \frac{D \cdot \Delta t}{k_B T}\mathbf{F} + \mathbf{S}, \tag{2}$$

where D is the translational diffusion coefficient for the relative motion and assumed to be spatially isotropic; $\mathbf{F}$ is the systematic inter-particle force, which is computed from the electrostatic field calculated before Brownian dynamics simulations; $k_B T$ is the Boltzmann constant times absolute temperature; and $\mathbf{S}$ is the stochastic component of the displacement arising from collisions of proteins with solvent molecules, which is generated by taking normally distributed random numbers obeying the relationship:

$$\langle \mathbf{S}^2 \rangle = 2D\Delta t$$

$$\langle \mathbf{S} \rangle = 0 \tag{3}$$

A similar equation governs the independent rotational Brownian motion of each particle, in which the force is replaced by a torque and D is replaced by an isotropic rotational diffusion coefficient D_{ir} for each particle i.

Next, BD simulations of MTX binding to the Kv1 channels were performed to identify the favorable complex(es). For simulations of protein-protein interactions, the two proteins were treated as rigid bodies. Therefore, the translational and rotational motions can be simulated for one of the proteins (protein II) around the other (protein I) (Gabdoulline and Wade, 1998) (Fig. 4). In this study we defined the larger protein, Kv1 channel, as protein I (i.e., the fixed protein) and the smaller protein, MTX, as protein II (i.e., the diffusing protein).

Trajectories were started with MTX at a random position and orientation on the b-surface (Fig. 4), a sphere of radius b (71 Å) centered on the Kv1 channels at which the forces due to the Kv1 channels are centrosymmetric. The mobile MTX was subject to three forces: the electrostatic attraction between the two proteins, the random Brownian force, and the frictional force due to solvent viscosity. The closest approach of the mobile protein MTX to the fixed receptor Kv1 channel was recorded, and the trajectory was terminated when the mobile ligand escaped the q-sphere (200 Å). The Bdtirm8.2 module (BD of two irregular rotating macromol-

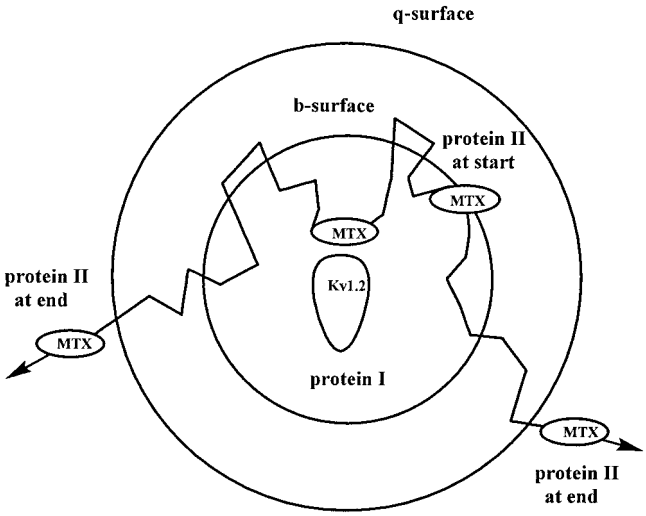

FIGURE 4 A systematic representation of the Brownian dynamics simulation of the association between scorpion toxin MTX and the Kv1.2 channel. Simulations were conducted in coordinates defined relative to the position of the center of the fixed protein, the Kv1.2 channel (protein I). At the beginning, each trajectory of the mobile protein (protein II), MTX, is positioned with a randomly chosen orientation at a randomly chosen point on the surface of the inner sphere of radius b (71 Å in this work). BD simulation is then performed until this protein diffuses outside the outer sphere of radius q (200 Å in this work). During the simulations, satisfaction of reaction criteria for encounter complex formation is monitored. The complexes with the smallest reaction distances were recorded.

ecules) of the MacroDox program was used to simulate the interactions between the scorpion toxin MTX and the Kv1 channel at pH 7.0 and 0.1 M ionic strength. All 35 structures of MTX in 1TXM were docked with the Kv1.1, Kv1.2, and Kv1.3 channels, respectively, typically by running 3000 trajectories for each MTX/channel combination. In addition to visual examination of the structures of the final complexes, statistical analyses were performed using the review module of MacroDox. We obtained the high occurence frequencies of key amino acid residues which formed intermolecular contacts between proteins in the complexes.

Structural refinement of the final complexes

To explore the mechanism of interaction of MTX and the Kv1 channel family in more detail, the final structure of the complex, obtained from BD simulations, was subjected to energy refinement using the adopted-basis Newton Raphson algorithm and the CHARMM22 force field in Quanta to relieve possible steric clashes and overlaps. During the structural refinement, a distance-dependent dielectric constant of 4 was used to simulate the solvation effect. The structure of this complex was subjected to energy minimization for 490 steps to achieve the gradient tolerance 0.05 kcal/mol^{-1} Å^{-1}. The details of the interactions were analyzed using the LIGPLOT program (McDonald and Thornton, 1994; Wallace et al., 1995).

RESULTS AND DISCUSSION

Electrostatic potentials

During the BD simulations, the proteins were treated as rigid bodies, so the effect of the flexibility of the proteins was not considered. To overcome this shortcoming, we considered all of the 35 available NMR conformations of the MTX scorpion toxin in solution when performing the BD simulations. For the Kv1 channels, because they are embedded in the membrane of the cell, they should not be substantially flexible.

The dipole moments together with the electrostatic calculations were visualized with the GRASP software (Nicholls et al., 1991). The potential maps were calculated with a simplified Poisson-Boltzmann solver, on the basis of an AMBER-derived parameter file. The appearance of the electrostatic potential on the surface of the Kv1.2 channel protein and the scorpion toxin MTX is given in Fig. 3. The mouth of the Kv1.2 channel, which is outside of the cell membrane, bears a large negative electrostatic potential that is centrosymmetric around the central axis of the Kv1.2 channel. The surface of MTX, on the contrary, has a large positive electrostatic potential, which comes mainly from the side chains of residues Lys23, Lys27, and Lys30 (Fig. 3 *B*). This suggests that MTX may associate with the entryway of the Kv1 channels using the positive patch around the side chains of Lys23, Lys27, and Lys30. This conclusion was validated by BD simulations (see discussion below). The resulting dipole moment of Kv1.2 is oriented along the symmetry axis due to the fourfold symmetry of the homotetramer and is oriented from the outer to the inner side of the membrane. It guides and orients the toxin into the pore, toward the binding site, and is thus responsible for the specificity. The orientation of the toxin is such that Lys23 in MTX protrudes into the Kv1.2 pore, interacting electrostatically with acidic residues, including Asp402, in the ion-selective filter. Both the electrostatic potential on the surface and dipole calculation show that the charge anisotropy is the driving force of the association of MTX to the Kv1 channels from the viewpoint of Coulombic interactions.

BD-identified MTX-Kv1.2 channel complexes

The center of mass of MTX and the position of the oxygen atom of the water in the selection filter of the x-ray crystallographic structure of KcsA were chosen as the monitors of association during the BD simulations. To avoid unfavorable complexes formed by MTX with the intracellular surface of the Kv1 channels, the separation defining a complex was set to 30 Å. This distance is large enough to obtain the most significant complexes from the simulations, as shown later.

During the initial BD runs, we found that the electrostatic attraction is so large that the simulations ran endlessly at pH 7.0, 0.1 M, and 298.15 K. When the binding patches of the two proteins are close to each other, the stochastic force is not large enough to overcome the electrostatic force, so MTX could not escape the binding site of the Kv1 channels. This was also found in our previous study (Cui et al., 2001, 2002). Two methods can be used to solve this problem: 1) simulate this system at sufficiently high salt concentration (the salt dampens the electrostatic field), so the interaction can be limited by the association rate rather than dissociation, and 2) increase the simulation temperature so as to make the stochastic force large enough to overcome the electrostatic force. The first approach is typically used when studying the reactive rate of the association of two proteins. The main purpose of this study was to obtain the complexes to aid in understanding the mechanism of the interaction between the two proteins. Therefore, we used the second approach, increasing the simulation temperature to 500 K, throughout all of the simulations.

BD simulations were performed for each conformation of MTX derived from the NMR studies (1TXM). The five MTX structures that docked most favorably with each Kv1 channel (i.e., favorable clusters with the highest probabilities) are listed in Table 1 along with their closest triplet contacts and the electrostatic interaction energy of each complex. The electrostatic interaction energies between MTX and Kv1 channels were calculated using the following process. The charges of MTX were assigned onto the electrostatic potential grids of each Kv1 channel, and then the electrostatic interaction energies were calculated by summing all the above assigned charges of MTX times the corresponding electrostatic potential values at the grids of the Kv1 channels (Madura et al., 1995; Zacharias et al., 1992).

Among the 35 conformations of MTX, the 10th, 23rd, 24th, 28th, and 33rd structures, which docked most favor-

TABLE 1 Possible triplet contacts between structures of MTX and Kv1 channels at the ionic strength of 0.1 M

Kv	MTX structure	Triplets (Kv channel residue-MTX residue)			F	E_{elec}
Kv1.1	10	D402(B)-K30	D402(C)-K23	E378(D)-K27	41	−20.6
		D402(A)-K30	D402(B)-K23	D402(C)-K7	83	−19.3
		D402(A)-K30	D402(B)-K23	H380(B)-K27	89	−19.3
	23	D402(B)-K30	D402(C)-K23	D402(D)-K7	73	−19.4
		D402(B)-K30	D402(C)-K23	E378(D)-K27	41	−20.6
	24	D402(C)-K27	D402(D)-K23	D402(B)-K30	69	−19.1
		D402(C)-K27	D402(D)-K23	D402(A)-K7	36	−19.3
		D402(C)-K27	D402(B)-K30	D402(A)-K7	36	−19.3
		D402(D)-K23	D402(B)-K30	D402(A)-K7	37	−19.2
	28	D402(C)-K27	D402(B)-V1	D402(D)-K30	26	−17.2
	33	D402(A)-K30	D402(D)-V1	E378(A)-K27	15	−17.1
Kv1.2	10	D402(C)-K23	D402(A)-K30	D378(C)-K27	104	−23.3
		D402(C)-K23	D402(D)-K7	D378(C)-K27	33	−23.2
		D402(C)-K7	D402(B)-K23	D402(A)-K30	138	−18.3
	23	D402(B)-K30	D402(C)-K27	D402(A)-K23	54	−20.0
	24	D402(C)-K27	D402(B)-K30	D402(D)-K23	38	−20.1
		D402(C)-K7	D402(B)-K23	D402(A)-K30	94	−18.2
		D402(B)-K23	D402(A)-K30	D378(C)-K27	82	−18.1
	28	D402(B)-K27	D402(C)-K30	D402(A)-V1	99	−19.1
	33	D402(B)-V1	D402(C)-K30	D378(C)-K27	27	−21.2
		D402(B)-V1	D402(C)-K23	D402(D)-K30	26	−21.4
		D402(C)-K23	D402(D)-K30	D378(C)-K27	26	−21.4
		D402(C)-K23	D402(D)-K30	R377(B)-K15	26	−21.0
Kv1.3	10	D402(D)-K30	H404(C)-K23	D386(B)-K27	28	−17.1
		H404(C)-K23	H404(B)-V1	D386(B)-K27	87	−17.1
		D402(C)-K30	D402(A)-K27	H404(C)-K23	21	−17.1
		D402(A)-K27	H404(D)-K23	D402(C)-K30	33	−16.3
	23	H404(B)-V1	D402(C)-K30	D402(B)-K27	59	−14.3
		D402(C)-K30	H404(A)-K23	D402(B)-K27	54	−14.7
	24	D402(A)-K27	H404(D)-K23	H404(B)-K7	77	−16.7
		D402(A)-K27	H404(D)-K23	H404(A)-K30	51	−16.7
		H404(D)-K23	H404(B)-K7	H404(A)-K30	59	−16.7
	28	D402(B)-K27	H404(C)-K30	H404(B)-V1	81	−15.2
	33	D402(B)-K27	H404(C)-K23	H404(B)-V1	34	−16.8
		H404(C)-K23	H404(B)-V1	D386(B)-K27	103	−16.7
		H404(C)-K23	H404(B)-V1	H404(A)-K30	61	−17.0

F, number of successfully docked complexes from 3000 attempts; E_{elec}, average electrostatic interaction energy between the two proteins (kcal/mol). A, B, C, and D represent the four chains of the Kv1.2 channel.

ably with the Kv1.1, Kv1.2, and Kv1.3 channels, had the highest frequencies (probabilities) of satisfying the criterion of association. The average electrostatic interaction energies between these five structures of MTX and Kv1 channels are −17∼−21 kcal/mol for Kv1.1, −19∼−24 kcal/mol for Kv1.2, and −15∼−17 kcal/mol for Kv1.3, respectively. The distribution of MTX (e.g., the 10th structure with the lowest electrostatic interaction energy) around the Kv1.2 channel is shown in Fig. 5, from which we can see that the largest distribution is the one in which the proteins are closer than 19 Å. This supports the selected interaction criterion.

To identify the favorable MTX-Kv1 channel complexes, we performed a detailed triplet contact analysis for each of the top five Kv1 channel complexes. The relative geometries of MTX-Kv1 channel complexes were defined by three close contact interactions, as only one or two are not sufficient. During this process we modified the criterion of the triplet contact of MacroDox. We analyzed the favorable triplet pairs between MTX and the Kv1 channels using a triplet contact distance of <5.5 Å. The distribution frequency and average electrostatic interaction of the five favorable complexes derived from this cycle of analysis are listed in Table 2. This tighter contact analysis shows that the average electrostatic interaction energies between the five structures of MTX and Kv1 channels are −17∼−21 kcal/mol for Kv1.1, −19∼−24 kcal/mol for Kv1.2, and −15∼−17 kcal/mol for Kv1.3, respectively, which is similar to the values in Table 1, although the distribution frequencies changed substantially in some cases. The 10th structure of MTX binds to the Kv1.2 channel with the highest frequency and the lowest average electrostatic interaction energy. The lowest electrostatic interaction energies between the 10th structure and Kv1 channels are

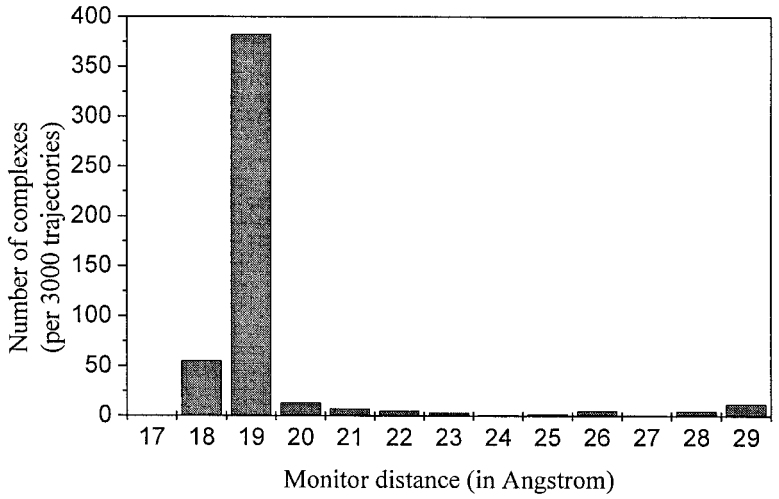

FIGURE 5 The distribution of distances between the two monitors for all complexes of the 10th structure of MTX associating with the Kv1.2 channel. (The monitor distances shorter than 30 Å were recorded.)

−20.9, −23.7, and −17.2 kcal/mol for Kv1.1, Kv1.2, and Kv1.3, respectively. The electrostatic interaction energy of the 10th structure of MTX with Kv1.2 is ~3 and 6 kcal/mol lower than that of Kv1.1 and Kv1.3, respectively; the frequency for matching the triplet contact criteria of Kv1.2 is much higher than that of Kv1.1 and Kv1.3 (Table 2), indicating that Kv1.2 is more sensitive to MTX than Kv1.1 and Kv1.3. Combining the electrostatic binding energies and the triplet matching frequencies, we can conclude that Kv1.2 is the most favorable channel for MTX binding among the three Kv1 channels, whereas the Kv1.1 channel is the intermediate one, and the Kv1.3 is the least favorable one. Our BD simulation results are in good agreement with the experiments on MTX, which show that MTX blocks the Kv1.1, Kv1.2, and Kv1.3 currents expressed in *Xenopus* oocytes with half-maximal blockage (IC_{50}) at 37, 0.8, and 150 nM (Blanc et al., 1997). Later on we will analyze in detail the intrinsic reason for this affinity difference at the molecular level. Our simulation also revealed that the 10th structure of MTX, among the 35 available structures in the PDB file, is the most favorable binding conformation for these Kv1 channels. This also indicates that the conformation of the proteins indeed affected the BD simulation results significantly.

As discussed above, the electrostatic interaction energies derived from BD simulations of MTX with Kv1 channels correlated well with their inhibitory activities, $R^2 = 0.88$ (Fig. 6). Nonelectrostatic interactions were not considered in the present BD simulations, as MacroDox has no function for calculating these interactions. To compensate for this energetic calculation deficiency and to validate the reasonability of the 3-D structural models of MTX-Kv1 complexes derived from BD simulations, the sophisticated energy function encompassed in the AutoDock program was used to predict the binding free energies of MTX with Kv1.1, Kv1.2, and Kv1.3. The AutoDock empirical binding free energy function contains a variety of interaction terms between a ligand and a receptor, including electrostatic interaction, van der Waals interaction, hydrogen-bonding interaction, and desolvation (hydrophobic) effects. It is sufficient for ranking different conformations of MTX and their association with different Kv1 channels. Using this energetic calculation paradigm, the binding free energies of MTX with Kv1.1, Kv1.2, and Kv1.3 channels were calculated, and the results are shown in Fig. 6. The binding free energies of MTX with the three Kv1 channels are −11.3, −13.2, and −10.9 kcal/mol, respectively. The AutoDock binding free energies have a good correlation with the experimental inhibitory activities ($-\log IC_{50}$) (Blanc et al., 1997), and $R^2 = 0.99$ (Fig. 6). These results demonstrate that the binding energies together with the distribution frequencies from BD simulations could be used as criteria to rank the binding conformations of MTX with Kv1 channels. Therefore, the structures of MTX-Kv1 complexes derived from the BD simulations are reasonable and practically represent the different interaction mechanism of MTX with Kv1 channels.

Contacts between MTX and Kv1.2 channel

Using BD simulations followed by triplet contact analyses, we identified the favorable complexes formed between MTX and the Kv1.2 channel. The BD trajectories of the 10th structure of MTX gave 491 candidate complexes with the Kv1.2 channel. The distribution of the centers of mass of the MTX structures around the Kv1.2 channel is presented in Fig. 7, which shows that MTX is located in the extracellular entryway of the Kv1.2 channel. This is in agreement with the electrostatic interaction calculations (Fig. 3).

We isolated the most stable structure having the strongest electrostatic interaction energy (−24.2 kcal/mol) and used it to analyze the contacts between MTX and the Kv1.2 channel. The structure of this complex was subjected to energy

TABLE 2 Possible triplet contacts for the top five complexes of MTX interacting with the Kv1 channels within a contact distance of 5.5 Å

Kv1	MTX Structure	Triplets (Kv1 channel residue-MTX residue)			F	E_{elec}
Kv1.1	10	D402(B)-K30	D402(C)-K23	E378(D)-K27	12	−20.9
		D402(A)-K30	D402(B)-K23	D402(C)-K7	28	−19.8
		D402(A)-K30	D402(B)-K23	H380(B)-K27	51	−20.1
	23	D402(B)-K30	D402(C)-K23	D402(D)-K7	7	−19.1
		D402(B)-K30	D402(C)-K23	E378(D)-K27	0	
	24	D402(C)-K27	D402(D)-K23	D402(B)-K30	4	−18.9
		D402(C)-K27	D402(D)-K23	D402(A)-K7	0	
		D402(C)-K27	D402(B)-K30	D402(A)-K7	0	
		D402(D)-K23	D402(B)-K30	D402(A)-K7	0	
	28	D402(C)-K27	D402(B)-V1	D402(D)-K30	4	−17.6
	33	D402(A)-K30	D402(D)-V1	E378(A)-K27	0	
Kv1.2	10	D402(C)-K23	D402(A)-K30	D378(C)-K27	92	−23.7
		D402(C)-K23	D402(D)-K7	D378(C)-K27	12	−23.4
		D402(C)-K7	D402(B)-K23	D402(A)-K30	0	
	23	D402(B)-K30	D402(C)-K27	D402(A)-K23	44	−20.0
	24	D402(C)-K27	D402(B)-K30	D402(D)-K23	12	−20.3
		D402(C)-K7	D402(B)-K23	D402(A)-K30	8	−19.0
		D402(B)-K23	D402(A)-K30	D378(C)-K27	12	−19.1
	28	D402(B)-K27	D402(C)-K30	D402(A)-V1	12	−19.3
	33	D402(B)-V1	D402(D)-K30	D378(C)-K27	6	−20.8
		D402(B)-V1	D402(C)-K23	D402(D)-K30	0	
		D402(C)-K23	D402(D)-K30	D378(C)-K27	24	−21.9
		D402(C)-K23	D402(D)-K30	R377(B)-K15	0	
Kv1.3	10	D402(D)-K30	H404(C)-K23	D386(B)-K27	33	−17.2
		H404(C)-K23	H404(B)-V1	D386(B)-K27	0	
		D402(C)-K30	D402(A)-K27	H404(C)-K23	0	
		D402(A)-K27	H404(D)-K23	D402(C)-K30	5	−16.3
	23	H404(B)-V1	D402(C)-K30	D402(B)-K27	0	
		D402(C)-K30	H404(A)-K23	D402(B)-K27	6	−15.1
	24	D402(A)-K27	H404(D)-K23	H404(B)-K7	0	
		D402(A)-K27	H404(D)-K23	H404(A)-K30	4	−16.3
		H404(D)-K23	H404(B)-K7	H404(A)-K30	2	−16.9
	28	D402(B)-K27	H404(C)-K30	H404(B)-V1	0	
	33	D402(B)-K27	H404(C)-K23	H404(B)-V1	0	
		H404(C)-K23	H404(B)-V1	D386(B)-K27	0	
		H404(C)-K23	H404(B)-V1	H404(A)-K30	0	

F, number of successfully docked complexes from 3000 attempts; E_{elec}, average electrostatic interaction energy between the two proteins (kcal/mol). A, B, C, and D represent the four chains of the Kv1.2 channel.

minimization for 490 steps to achieve the gradient tolerance 0.05 kcal/mol^{-1} Å^{-1}) using the adopted-basis Newton Raphson algorithm and the CHARMM22 force field as implemented in the Quanta program. The optimized structure of the complex is shown in Fig. 8. In general, the scorpion toxin binds to the K^+ channel mainly via its β-sheet, although a few scorpion toxins such as P05 binds to the K^+ channel mainly via its α-helix rather than its β-sheet. Despite the unusual disulfide bridge motif, the binding of MTX to Kv1.2 belongs to the first situation, i.e., mainly via its two antiparallel β-sheets, whereas its α-helix is far away from the interaction surface of the Kv1 channel. This is similar to most scorpion toxins such as charydbotoxin (CTX) with only three disulfide bridges and in agreement with the experiment of Fajloun et al. (2000a) and Avdonin et al. (2000). Our BD simulation result shows that the critical residues of MTX for recognizing the Kv1.2 channel are three lysine residues, Lys23, Lys27, and Lys30. Among them, Lys23 and Lys30 are located in the two antiparallel β-sheets of MTX, respectively, with the greatest positive potential. Lys23 protrudes into the pore of Kv1.2 (Fig. 8 *A*), and Lys27 is located in the β-turn. The principal MTX-Kv1.2 channel interactions derived from the refined structure were analyzed and displayed using the LIGPLOT program (McDonald and Thornton, 1994; Wallace et al., 1995), shown in Fig. 9. The hydrogen bonds and hydrophobic contact parameters presented in the refined complex are listed in Tables 3 and 4, respectively. Six hydrogen bonds are formed between MTX and the Kv1.2 channel: two from Lys23 (MTX) with Gly401(D) and Tyr400(C) (Kv1.2), one from Tyr32 (MTX) with Asp402 (D) (Kv1.2), two from Lys27 (MTX) with Thr406(C) and Asp378(C) (Kv1.2), and one from Lys30 with Asp402(A) (Table 3 and Fig. 9). Five hydrophobic contacts are formed between MTX and the

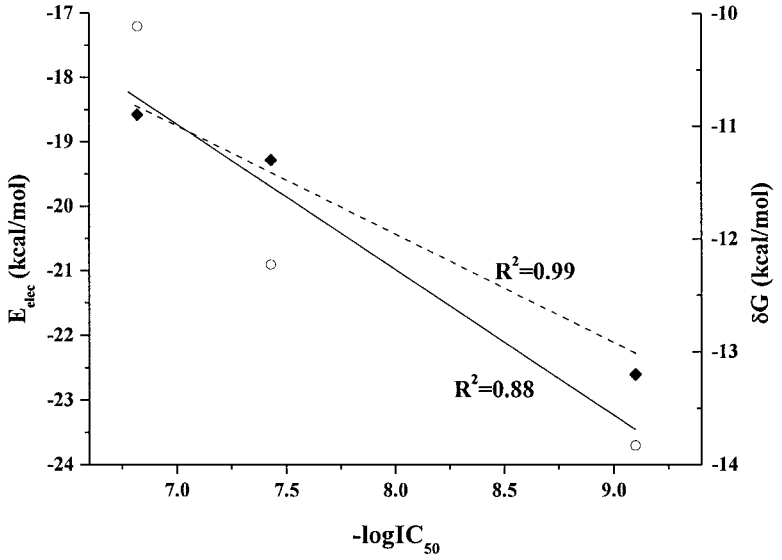

FIGURE 6 Relationship between the interaction energies and the inhibitory activities ($-\log IC_{50}$) of MTX with Kv1 channels. The left axis represents the electrostatic interaction energies of MTX with Kv1.1, Kv1.2, and Kv1.3 derived from BD simulations (real line with the $R^2 = 0.88$), whereas the right axis represents the AutoDock results for the binding free energies of MTX with the same Kv1 channels (*dashed line* with $R^2 = 0.99$)

Kv1.2 channel: two for Lys30(MTX) with Asp402(A), one for Lys32 with Val404(A), one for Lys23 with Gly401(C), and one for Pro20 with Arg377(A) (Table 4 and Fig. 9). The refined structure of the complex has favorable electrostatic interactions between the two proteins: three positive lysine residues of MTX interact with three negative aspartic acid residues of the Kv1.2 channel through strong electrostatic interactions.

It indicates that, despite a nonconventional disulfide pattern, the structure of MTX remains similar to that of other toxins such as CTX and kaliotoxin (KTX) (Blanc et al., 1997). Comparison of the 3-D structures of MTX and CTX shows that, on the whole, they adopt a common structural motif, the α/β scaffold, which is an α-helix connected to a double stranded β-sheet by two disulfide bridges. The structural alignment between MTX and CTX has been carried by Avdonin et al. (2000), who showed that the Cα deviations are typically less than 2 Å. Previous analysis of mutants of CTX and their relative binding to *Shaker* channels (Goldstein et al., 1994) allowed the identification of residues directly involved in the interaction of the toxin with a voltage-gated potassium channel. Five residues, Lys27, Met29, Asn30, Arg34, and Tyr36, in CTX are well conserved among different K^+ channel toxins and are considered critical for binding to the receptor, because their mutation induces a dramatic drop in activity. These residues correspond to Lys23, Ile25, Asn26, Lys30, and Tyr32 in MTX. The triplet contact analyses from our BD simulation results show that the important triplets are Lys23(MTX)-Asp402(C)(Kv1.2), Lys27(MTX)-Asp378(C)(Kv1.2), and Lys30(MTX)-Asp402(A)(Kv1.2) (Table 2). Lys23 is essential for the interaction of MTX with the Kv1.2 channel and is therefore in line with the observation that this lysine plays a role similar to that of Lys27 in CTX, which is known to protrude into the pore and interact with the residue of the pore region (Goldstein et al., 1994). This residue forms two hydrogen bonds with the carbonyl groups of the backbones of Gly401(D) and Tyr400(C) and one hydrophobic contact with the Gly401(C) of Kv1.2 channel. Lys23 (MTX), Gly401 (Kv1.2), and Tyr400 (Kv1.2) are very conserved in the scorpion toxin or Kv1 channels (Blanc et al., 1997; Goldstein et al., 1994; Miller, 1995; Heginbotham et al., 1992, 1994). The importance of Lys23 was also highlighted by the mutation Lys23Ala (K23A) (Carlier et al., 2000), which showed a 1000-fold decreased toxin affinity. Lys27, which is located at the loop between the two β-sheets, is also critical for the binding of MTX to the Kv1.2 channel: it forms two hydrogen bonds with the carbonyl groups of the backbones of Thr406(C) and Asp378(C) of Kv1.2.

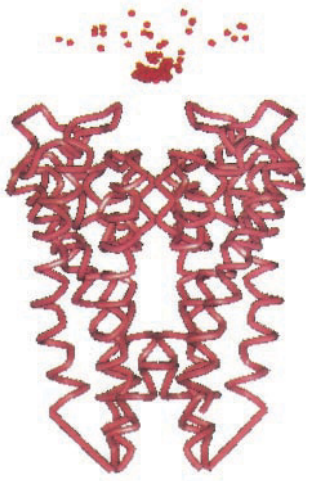

FIGURE 7 Distribution of the 10th structure of MTX around the extracellular mouth of the Kv1.2 channel. The Kv1.2 channel is represented as a C_α trace. Each dot represents the center of mass of MTX in an encounter snapshot with the Kv1.2 channel.

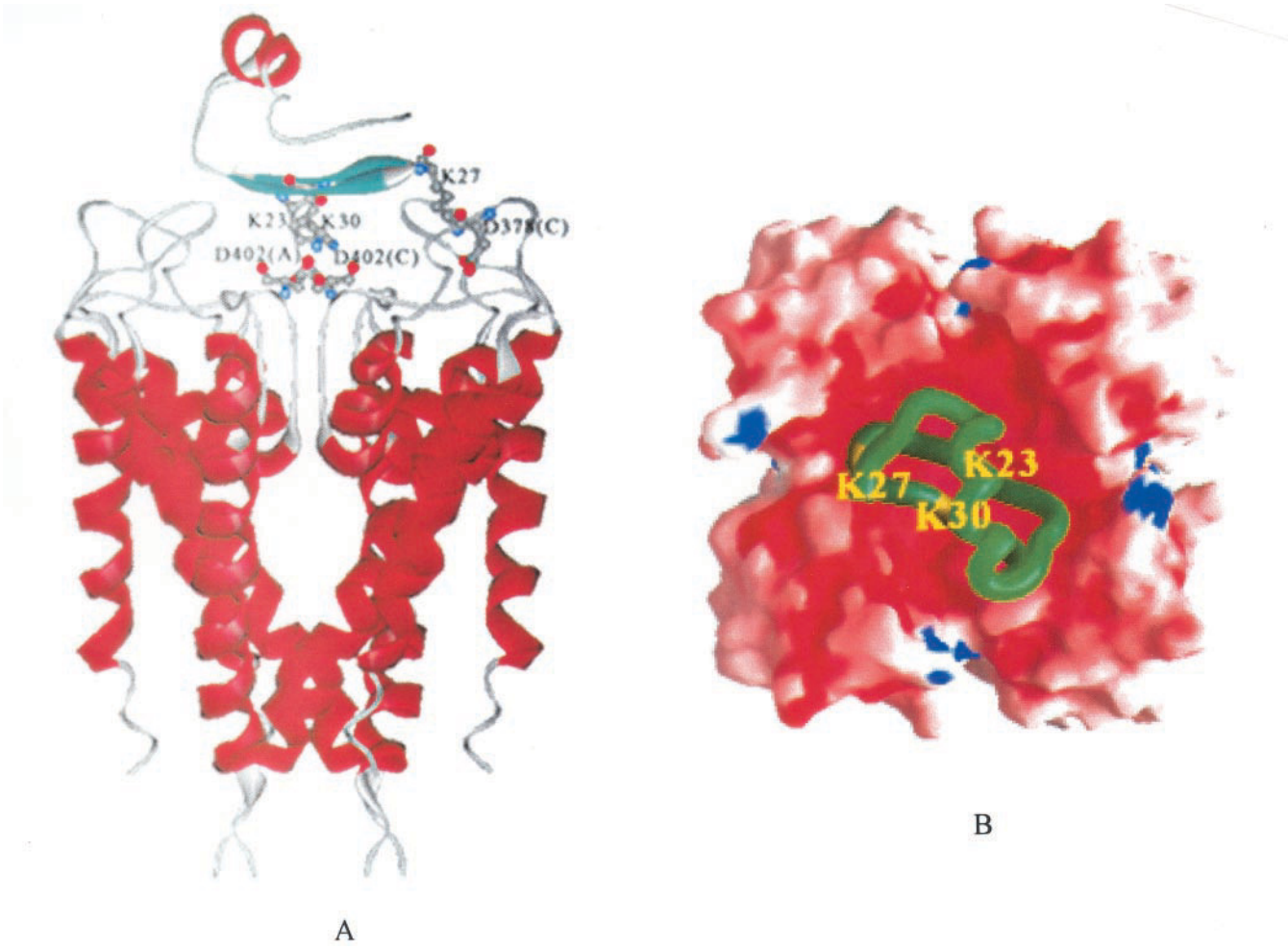

FIGURE 8 A typical final complex of the 10th structure of MTX and the Kv1.2 channel. (*A*) The two molecules are represented as ribbon structures. The closest contacts are Lys23-Asp402(C), Lys30-Asp402(B), and Lys27-Asp378(C). (*B*) The top view of the complex shown in *A*, which was generated with the program GRASP (Nicholls et al., 1991). The Kv1.2 channel is represented as a molecular surface color coded by electrostatic potential and MTX as a green worm-like structure.

Kharrat et al. (1996) and Avdonin et al. (2000) also highlighted the importance of this residue and indicated that Lys27 could be involved in the Kv channel recognition. Lys30 in MTX is the counterpart of Arg34 in CTX; it binds to the backbone carbonyl groups of Asp402(A) through one hydrogen bond and two hydrophobic contacts. The influence of the Arg34Lys (R34K) mutation in CTX on the pharmacological activity of the *Shaker* K^+ channel is weak (only a 3-fold drop), whereas both Arg34Asp (R34D) and Arg34Glu (R34E) mutations result in dramatic decreases (more than a 3700-fold drop) in the pharmacological activities (Goldstein et al., 1994). All these show the importance of lysine or arginine at this position in MTX or CTX for the binding affinity of the Kv channel or *Shaker* channel. However, the importance of Lys30 of MTX, which has been shown by our BD simulations with comparing the mutation and binding assay of CTX with the *Shaker* K^+ channel, has not been appreciated in previous experiments. Interestingly, the side chains of Lys23 and Lys30 in the MTX-Kv1.2 complex are at the surface of the β-sheet, close in space to each other (Fig. 8 *A*), forming a positively charged surface on the β-sheet. Furthermore, these side chains are rather flexible and are generally exposed to solvent when MTX stays in the solution alone. Therefore, it is worthwhile to perform a mutation study on Lys30. Residue Tyr32 also plays an important role: our simulation results indicate that it interacts with Asp402(D) through one hydrogen bond and with Val404(A) through one hydrophobic contact. In addition, BD simulations and structural optimizations could not identify the role of Ile25 and Asn26 in MTX. However, this could be explained through the structural alignment between MTX and CTX by Avdonin et al. (2000), which indicates that Ile25 and Asn26 in MTX show a considerable divergence from the corresponding Met29 and Asn30 in CTX. Compared with the five important residues in CTX, Lys23, Lys30, and Tyr32 in MTX play similar critical roles.

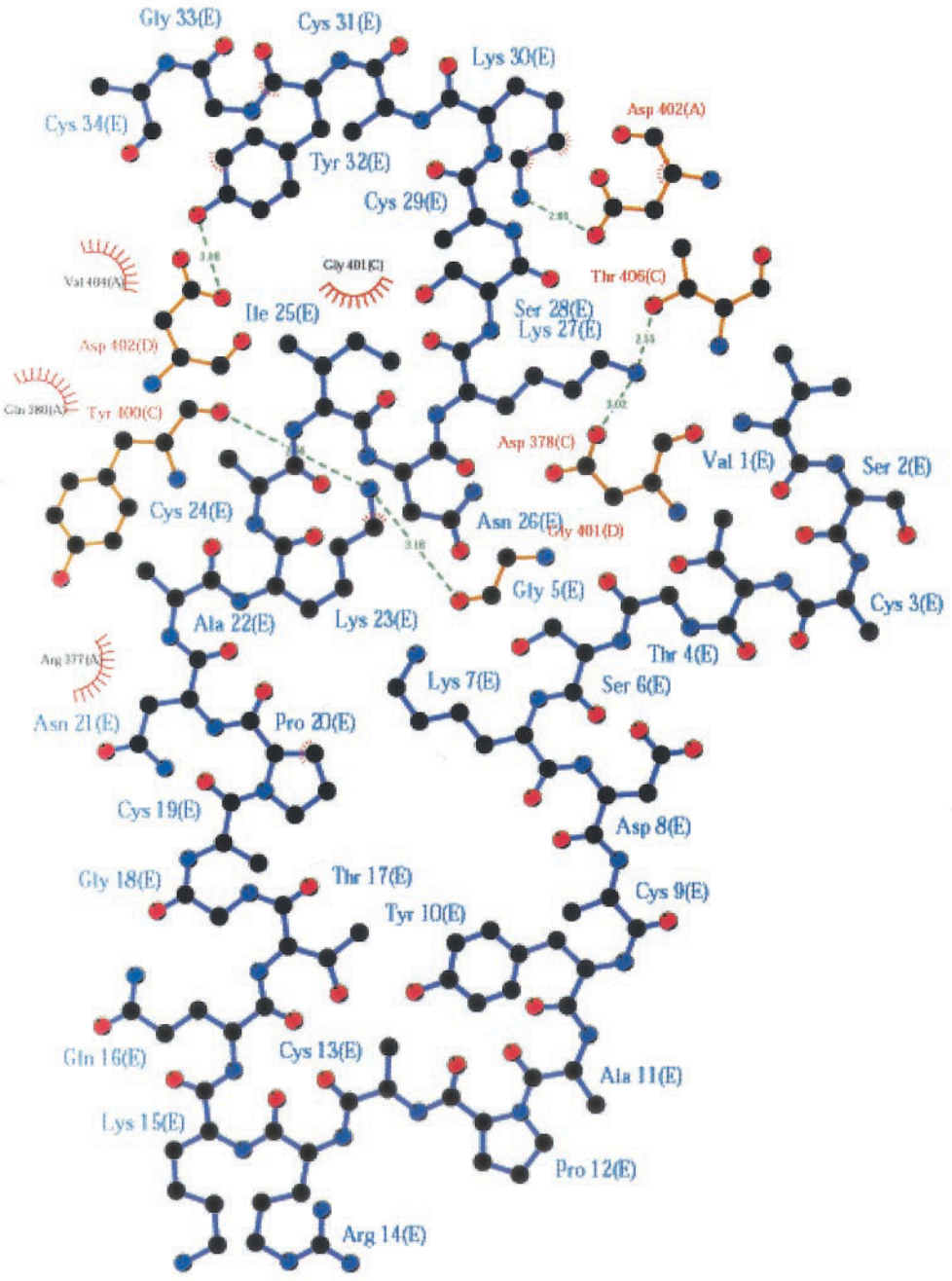

FIGURE 9 Schematic depiction (generated by LIGPLOT) of the main interactions between the scorpion toxin MTX and the Kv1.2 channel.

TABLE 3 Hydrogen bonds between the MTX scorpion toxin and the Kv1.2 channel in the MTX-Kv1.2 channel complex

Scorpion toxin MTX		Kv1.2 channel		
Residue	Atom	Residue	Atom	Distance (Å)
TYR32	OH	ASP402(D)	OD1	3.08
LYS23	NZ	GLY401(D)	O	3.18
LYS27	NZ	THR406(C)	OG1	2.55
LYS23	NZ	TYR400(C)	O	2.66
LYS27	NZ	ASP378(C)	OD2	3.02
LYS30	NZ	ASP402(A)	OD1	2.86

The 3-D model of the complex was constructed based on the BD simulations and molecular mechanics structural refinement for the 10th structure of MTX associating with the Kv1.2 channel. A, B, C, and D represent the four chains of the Kv1.2 channel.

TABLE 4 Hydrophobic contacts between the MTX scorpion toxin and Kv1.2 channel in the MTX-Kv1.2 channel complex

Scorpion toxin MTX		Kv1.2 channel		
Residue	Atom	Residue	Atom	Distance (Å)
LYS30	CD	ASP402(A)	CA	3.87
LYS30	CE	ASP402(A)	CA	3.81
TYR32	CE2	VAL404(A)	CG1	3.57
LYS23	CE	GLY401(C)	C	3.63
PRO20	CB	ARG377(A)	C	3.98

The 3-D model of the complex was constructed based on the BD simulations and molecular mechanics structural refinement for the 10th structure of MTX associating with the Kv1.2 channel. A, B, C, and D represent the four chains of the Kv1.2 channel.

However, Ile25 and Asn26 contribute little to the binding site recognition. On the other hand, what is interesting is that Lys27, which corresponds to Lys30 in CTX, plays a more important role in MTX. It is also likely that changes in half-cysteine pairings may contribute to conformational alterations and repositioning of key residues involved in toxin activity.

During the four years since the 3-D structure of MTX was characterized, research was focused on the pharmacological activity of MTX because of its unique disulfide bridge motif. The point mutations on residues Pro12, Pro20 (Carlier et al., 2001), Arg14, Lys15, Gly33 (Fajloun et al., 2000b), Cys19, and Cys34 (Fajloun et al., 2000a) result in disulfide bridge reorganization and alter the pharmacological activity more or less, whereas few mutant cycle experiments on conserved residues have been reported due to lack of significant theoretical guidance. The maintenance of a toxin conformation may account for the ability of MTX to recognize Kv1 channels. Complementary mutations in both the channel and the toxin structures would provide valuable insights into MTX's mechanism of action. Bontems et al. (1992) have indicated the mutation of Lys27, Arg34, and Tyr36 do not alter the conserved structure of CTX. For MTX, future toxin-directed point mutation studies will aim to alter the residues (Lys27, Lys30, and Tyr32) and analyze the effects of altering the lateral chain of Lys23 on the mode of action.

For Kv1.2, the BD simulations and structural optimizations indicate that each of the negatively charged residues Asp402(A-D) from the four symmetric subunits of Kv1.2 plays an essential role in the recognition of MTX; this is similar to the recognition of KTX by Kv1.3 (Aiyar et al., 1995). Analyzing the interaction of KTX and CTX with Kv1.3 will be helpful in understanding the recognition of MTX with Kv1 channels. The alignment of MTX, KTX, and CTX is shown in Fig. 10 *A*. Aiyar et al. (1995) have

FIGURE 10 (*A*) The sequence alignment of MTX, CTX, and KTX. The conserved residues are highlighted. (*B*) The sequence alignment of KcsA, Kv1.1, Kv1.2, Kv1.3, and *Shaker* B potassium channel.

TABLE 5 Electrostatic interaction energies (kcal/mol) from the methods of the test charges and the FDPB

Kv1	MTX structure	Triplets	Test charge	FDPB
Kv1.2	10	D402(C)-K23	−24.2	−25.1
		D402(A)-K30	−23.8	−24.3
		D378(C)-K27	−23.9	−24.9
		D402(C)-K23	−23.4	−24.1
		D402(D)-K7	−23.1	−23.7
		D378(C)-K27	−22.9	−21.9
	23	D402(B)-K30	−20.5	−22.2
		D402(C)-K27	−20.0	−22.5
		D402(A)-K23	−20.0	−22.0
	24	D402(C)-K27	−20.2	−21.8
		D402(B)-K30	−20.2	−22.1
		D402(D)-K23	−20.0	−22.6
		D402(C)-K7	−19.1	−20.5
		D402(B)-K23	−19.1	−20.2
		D402(A)-K30	−18.7	−20.3
		D402(B)-K23	−19.2	−20.4
		D402(A)-K30	−19.1	−21.2
		D378(C)-K27	−18.8	−20.9
	28	D402(B)-K27	−19.1	−20.4
		D402(C)-K30	−19.3	−20.3
		D402(A)-V1	−19.2	−20.2
	33	D402(B)-V1	−21.1	−21.5
		D402(D)-K30	−20.8	−19.7
		D378(C)-K27	−20.9	−19.5
		D402(C)-K23	−22.1	−21.9
		D402(D)-K30	−21.9	−22.3
		D378(C)-K27	−21.8	−22.9
Kv1.1	10	D402(B)-K30	−20.4	−21.8
		D402(C)-K23	−19.7	−22.0
		E378(D)-K27	−20.8	−21.5
		D402(A)-K30	−19.1	−20.2
		D402(B)-K23	−19.1	−20.0
		D402(C)-K7	−19.7	−20.4
		D402(A)-K30	−19.7	−20.0
		D402(B)-K23	−19.8	−19.9
		H380(B)-K27	−20.4	−20.1
Kv1.3	10	D402(D)-K30	−17.3	−18.6
		H404(C)-K23	−16.9	−17.9
		D386(B)-K27	−16.4	−18.5
		D402(A)-K27	−16.6	−17.2
		H404(D)-K23	−16.4	−17.3
		D402(C)-K30	−16.2	−17.7

demonstrated that Trp14 and Lys31 in CTX and Leu15 and Arg31 in KTX are close to Gly380 in Kv1.3, which plays a vital role in the interaction with CTX and KTX. Gly380 is the counterpart of Phe425 in *Shaker* B (the alignment of Kv1 channels and the *Shaker* B channel was generated by Insight II 2000 and shown in Fig. 10 *B*). Goldstein et al. (1994) suggested that the single point mutation Phe425Gly (F425G) strengthened the affinity of CTX for *Shaker* B by 2000-fold and that the blockage might depend on the size of the amino acid at this position. This conclusion is also validated by the mutation experiment of CTX on Kv1.3 (Aiyar et al., 1995), which shows that the Gly380Gln (G380Q) mutation makes Kv1.3 resistant to CTX, whereas we noticed that the MTX-sensitive Kv1.2 (IC_{50} = 0.8 nM) (Blanc et al., 1997) has a glutamine at the homologous position (Fig. 10 *B*). We will now analyze this in detail at the molecular level. We mentioned above that the residues Trp14 and Lys31 in CTX and Leu15 and Arg31 in KTX interact with Gly380 in Kv1.3. Fig. 10 *A* shows that Tyr10 in MTX corresponds to Trp14 in CTX and Leu15 in KTX. The residue at this position is not conserved, although Lys27 in MTX corresponds to Lys31 in CTX and Arg31 in KTX; this residue is conserved. Our triplet analyses of the BD simulations show that Lys27 in MTX interacts with Asp378 in Kv1.2 (Table 2). This indicated that Asp378 is the critical residue involved in the recognition of MTX. Kv1.1 has a negatively charged glutamic acid and Kv1.3 has a neutral serine at the homologous position (Asp378 in Kv1.2) (Fig. 10B). Thus, we can rationalize why MTX is more active on Kv1.2 than on the Kv1.1 and Kv1.3 potassium channels. Future mutant cycle experiments to determine the relative importance of the residues Asp378 in Kv1.2 will be of particular interest.

CONCLUSION

We have obtained a reasonable 3-D model of the MTX-Kv1.2 channel complex through BD simulations and molecular mechanics structural refinement (Fig. 8). BD simulations predict that the β-sheet of MTX associates with the extracellular entryway of the Kv1 channel, which is in line with the primary clues from the electrostatic interaction calculations (Fig. 3) and mutagenesis results (Carlier et al., 2000). Our docking process overcame some of the disadvantages of BD; i.e., it cannot easily consider the conformational flexibility of the associating proteins. We noticed that the conformation indeed affected the simulation results. Triplet contact analyses using modified criteria, along with electrostatic interaction energy calculations, further demonstrated that the 10th structure in 1TXM is the best conformation for the scorpion toxin MTX to bind with the Kv1 channels. Although Kv1.1, Kv1.2, and Kv1.3 have very similar pore structures, they display different affinities for the MTX toxin. We aligned their sequences and found that their amino acid residue compositions in the vestibule are not conserved. Our 3-D model of the MTX-Kv1.2 channel complex constructed with the results of BD simulations followed by molecular mechanics structural refinement can reasonably explain the affinity difference of MTX with Kv1 (Kv1.1, Kv1.2, and Kv1.3) channels. In addition, both BD simulations and molecular mechanics refinement indicate that residue Asp378 of the Kv1.2 channel is critical for both the recognition and the binding of MTX to the Kv1.2 channel, which has not been identified in previous experiments. Future toxin-directed point mutation studies may aim to alter the residues Lys27, Lys30, and Tyr32 of MTX and Asp378 of the Kv1.2 channel and analyze the effect of altering the lateral chain of Lys23 on the mode of action.

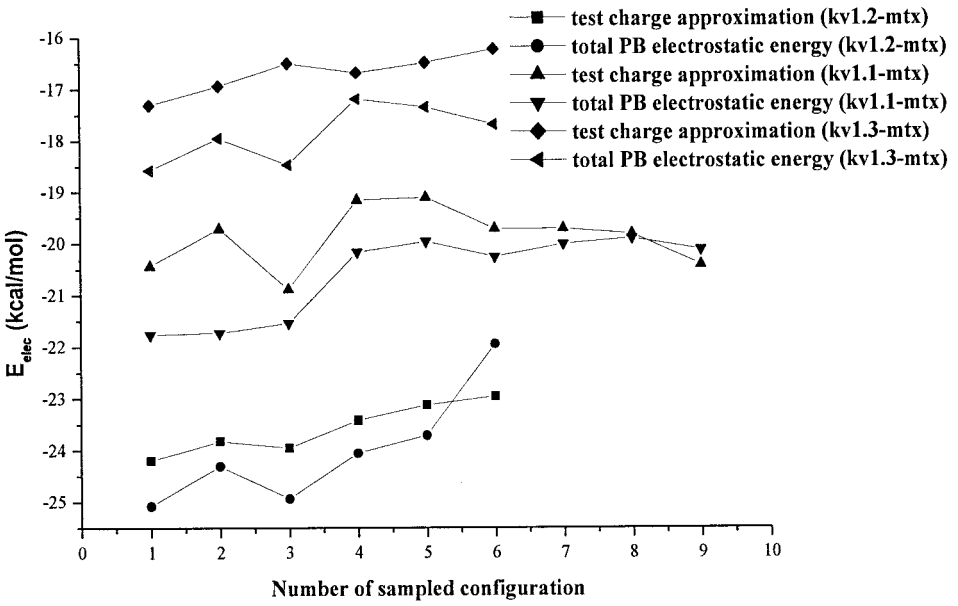

FIGURE 11 Electrostatic interaction energies for the 10th conformation of MTX with Kv1.1, Kv1.2, and Kv1.3.

The consistency between the results of the BD simulations and the experimental data indicated that our 3-D model of the MTX-Kv1.2 channel complex is reasonable and can be used in future biological studies, such as rational design of the blocking agents of Kv1.2 channels and mutagenesis in both toxin and Kv1 channels.

APPENDIX

The MacroDox program uses a test charge approach during BD simulation where atomic partial charges are assigned to the moving molecule. This may give rise to errors in calculating the electrostatic interaction energy because of its weak representation of the electrostatic potential. However, solution of the finite-difference Poisson-Boltzmann (FDPB) equation to obtain the interaction energies between the proteins at each step of the thousands of BD trajectories is not currently computationally feasible. To demonstrate the feasibility of the test charge approach in treating the MTX-Kv1 channel interactions, especially in calculating the electrostatic interaction energy, the UHBD program (Madura et al., 1994, 1995) was applied to calculate the intermolecular electrostatic interaction energies with high accuracy by numerical solution of the finite-difference linearized Poisson-Boltzmann equation for some sampled configurations. Partial atomic charges and atomic radii were assigned from the CHARMM22 parameter set. The protonation states of each titratable residue were assigned according to the Tanford-Kirkwood calculation at pH 7.0 and ionic strength 0.1 M. All the other parameters are the same as those adopted in the MacroDox calculations. For each triplet listed in Table 2, three lowest-energy configurations were sampled, and the electrostatic interaction energies calculated by using the test charge treatment and the FDPB equation method are listed in Table 5 and also shown in Fig. 11. The FDPB results indicate that the 10th conformation of MTX binds to Kv1 channels with the lowest electrostatic interaction energy, which is in agreement with the test charge result. Moreover, the lowest electrostatic interaction energies of FDPB between the 10th conformation of MTX and Kv1.1, Kv1.2, and Kv1.3 are −21.8, −25.1, and −18.6 kcal/mol, respectively, adopting the same sequence as from the test charge approximation; i.e., Kv1.2 is the most favorable channel for MTX binding among the three Kv1 channels, whereas the Kv1.1 channel is the intermediate one, and the Kv1.3 is the least favorable one. Although the absolute data of the test charge approximation is different from that of FDPB (Table 5), the trends are similar (Fig. 11), and the two sets of data correlate well with each other, $R^2 = 0.80$ (Fig. 12). Furthermore, it has been verified that the BD simulations resulting from the test charge approximation produced reasonable results for the interactions of scorpion toxin Lq2 binding with *Shaker* K^+ channel (Cui et al., 2001) and of toxin P05 binding with the small-conductance calcium-activated (SK) potassium channel (Cui et al., 2002). All of these studies indicate that the test charge treatment is suitable for studying Kv1-MTX interactions and their mutual recognition.

In addition, the main purpose of this paper was to study the recognition of the unique toxin MTX with four disulfide bonds with Kv1 channels rather than accurate association rate calculations or accurate binding energies. Therefore, we used the test charge approach during the BD simulation in this study.

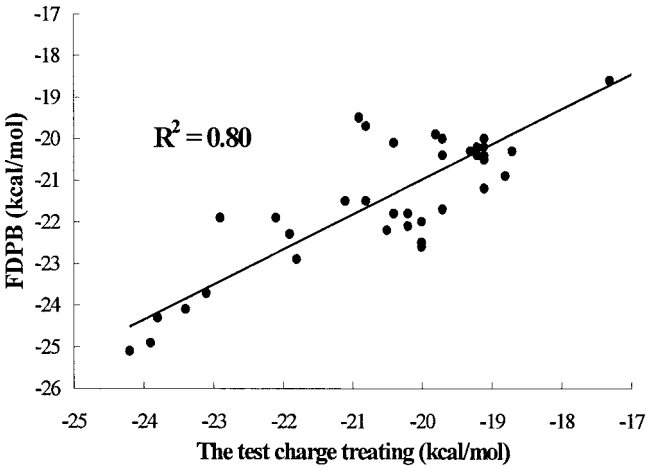

FIGURE 12 Correlation of the electrostatic interaction energies between the test charge results and the FDPB results for the sampled configurations in Table 5. These encounter complexes are obtained from the BD simulations.

We thank Prof. S. H. Northrup for his kindness in offering us the MacroDox 3.2.2 program and his helpful discussions.

We gratefully acknowledge financial support from the National Natural Science Foundation of China (grant 29725203), the State Key Program of Basic Research of China (grant 1998051115), Life Science Foundation for Young Scientists of Chinese Academy of Sciences (grant STZ-00–06), Qi Ming Xiang Foundation of Shanghai Ministry of Science and Technology (grant 00QB14034), 863 Hi-Tech Project (grants 2001AA235041 (X.L., 863) and 2001AA235051 (J.S., 863)). The calculations were performed on an Origin 3200 at the Center for Drug Discovery and Design, State Key Laboratory of Drug Research, Shanghai Institute of Meteria Medica.

REFERENCES

Aiyar, J., J. M. Withka, J. P. Rizz, D. H. Singleton, G. C. Andrews, W. Lin, J. Boyd, D. C. Hanson, M. Simon, B. Dethlefs, C. Lee, J. E. Hall, G. A. Gutman, and K. G. Chandy. 1995. Topology of the pore-region of a K^+ channel revealed by the NMR-derived structures of scorpion toxins. *Neuron.* 15:1169–1181.

Avdonin, V., B. Nolan, J. M. Sabatier, M. D. Waard, and T. Hoshi. 2000. Mechanisms of maurotoxin action on *Shaker* potassium channels. *Biophys. J.* 79:776–787.

Bernstein, F. C., T. F. Koetzle, G. J. Williams, E. E. Meyer, Jr., M. D. Brice, J. R. Rodgers, O. Kennard, T. Shimanouchi, and M. Tasumi. 1977. The Protein Data Bank: a computer-based archival file for macromolecular structures. *J. Mol. Biol.* 112:535–542.

Blanc, E., J. M. Sabatier., R. Kharrat, S. Meunier, M. E. Ayeb, J. V. Rietschoten, H. Darbon. 1997. Solution structure of maurotoxin, a scorpion toxin from *Scorpio maurus*, with high affinity for voltage-gated potassium channels. *Proteins.* 29:321–333.

Bontems, F., B. Gilquin, C. Roumestand, A. Ménez, and F. Toma. 1992. Analysis of side-chain organization on a refined model of charybdtoxin: structural and functional implications. *Biochemistry.* 31:7756–7764.

Brandt, T., and M. Strupp. 1997. Episodic ataxia type 1 and 2 (familial periodic ataxia/vertigo). *Audiol. Neuro-Otol.* 2:373–383.

Carlier, E., V. Avdonin, S. Geib, Z. Fajloun, R. Kharrat, H. Rochat, J. M. Sabatier, T. Hoshi, and M. D. Waard. 2000. Effect of maurotoxin, a four disulfide-bridged toxin from the chactoid scorpion *Scorpio maurus*, on *Shaker* K^+ channels. *J. Peptide Res.* 55:419–427.

Carlier, E., Z. Fajloun, P. Mansuelle, M. Fathallah, A. Mosbah, R. Oughideni, G. Sandoz, E. D. Luccio, S. Geib, I. Regaya, J. Brocard, H. Rochat, H. Darbon, C. Devaux, J. M. Sabatier, and M. D. Waard. 2001. Disulfide bridge reorganization induced by proline mutations in maurotoxin. *FEBS Lett.* 489:202–207.

Chandy, K. G., and G. A. Gutman. 1995. Voltage-gated K^+ channel genes. *In* Handbook of Receptors and Channels: Ligand and Voltage-Gated Ion Channels. A. North, editor. CRC Press, Boca Raton, FL. 1–71

Cui, M., J. H. Shen, M. Briggs, W. Fu, J. J. Wu, Y. M. Zhang, X. M. Luo, Z. W. Chi, R. Y. Ji, H. L. Jiang, and K. X. Chen. 2002. Brownian dynamics simulations of the recognition of the scorpion toxin P05 with the small conductance calcium-activated potassium channels. *J. Mol. Biol.* 318:417–428.

Cui, M., J. H. Shen, J. M. Briggs, X. M. Luo, X. J. Tan, H. L. Jiang, K. X. Chen, and R. Y. Ji. 2001. Brownian dynamics simulations of interaction between scorpion toxin Lq2 and potassium ion channel. *Biophys. J.* 80:1659–1669.

Darbon. H., E. Blanc, and J. M. Sabatier. 1999. Three-dimensional structure of scorpion toxins: towards a new model of interaction with potassium channels. *In* Perspectives in Drug Discovery and Design: Animal Toxins and Potassium Channels. H. Darbon and J. M. Sabatier. editors. Kluwer, Dordrecht, The Netherlands. 15:40–60.

Doyle, D. A., J. M. Cabral, R. A. Pfuetzner, A. Kuo, J. M. Gulbis, S. L. Cohen, B. T. Chait, and R. MacKinnon. 1998. The structure of the potassium channel: molecular basis of K^+ conduction and selectivity. *Science.* 280:69–77.

Ermak, D. L., and J. A. McCammon. 1978. Brownian dynamics with hydrodynamic interactions. *J. Chem. Phys.* 69:1352–1360.

Fajloun, Z., G. Ferrat, E. Carlier, M. Fathallah, C. Lecomte, G. Sandoz, E. D. Luccio, K. Mabrouk, C. Legros, H. Darbon, H. Rochat, J. M. Sabatier, and M. D. Waard. 2000a. Synthesis, ^1H NMR structure, and activity of a three-disulfide-bridged maurotoxin analog designed to restore the consensus motif of scorpion toxins. *J. Biol. Chem.* 275: 13605–13612.

Fajloun, Z., A. Mosbah, E. Carlier, P. Mansuelle, G. Sandoz, M. Fathallah, E. D. Luccio, C. Devaux, H. Rochat, H. Darbon, M. D. Waard, and J. M. Sabatier. 2000b. Maurotoxin versus Pi1/HsTx1 scorpion toxins: toward new insights in the understanding of their distinct disulfide bridge patterns. *J. Biol. Chem.* 275:39394–39402.

Gabdoulline, R. R., and R. C. Wade. 1998. Brownian dynamics simulation of protein-protein diffusional encounter. *Methods.* 14:329–341.

Goldstein, S. A. N., and T. J. Colatsky. 1996. Ion channels: too complex for rational drug design? *Neuron.* 16:913–919.

Goldstein, S. A. N., D. J. Pheasant, and C. Miller. 1994. The CTX receptor of a *Shaker* K channel: peptide and channel residues mediating molecular recognition. *Neuron.* 12:1377–1388.

Grissmer, S., A. N. Nguyen, J. Aiyar, D. C. Hanson, R. J. Mather, G. A. Gutman, M. J. Karmilowicz, D. D. Auperin, and K. G. Chandy. 1994. Pharmacological characterization of five cloned voltage-gated K^+ channels, types Kv1.1, 1.2, 1.3, 1.5, and 3.1, stably expressed in mammalian cell lines. *Mol. Pharmacol.* 45:1227–1234.

Heginbotham, L., T. Abramson, and R. MacKinnon. 1992. A functional connection between the pores of distantly related ion channels as revealed by mutant K^+ channels. *Science.* 258:1152–1155.

Heginbotham, L., Z. Lu, T. Abramson, and R. MacKinnon. 1994. Mutations in the K^+ channel signature sequence. *Biophys. J.* 66:1061–1067.

Hoshi, T., Z., W. N. Zagotta, and R. W. Aldrich. 1990. Biophysical and molecular mechanisms of shaker potassium channel inactivation. *Science.* 250:533–538.

Kaczorowski, G. J., and M. L. Garcia. 1999. Pharmacology of voltage-gated and calcium-activated potassium channels. *Curr. Opin. Chem. Biol.* 3:448–458.

Kharrat, R., K. Mabrouk, M. Crest, H. Darbon, R. Oughideni, M. F. Martin-Eauclaire, G. Jacquet, M. E. Ayeb, J. V. Rietschoten, H. Rochat, and J. M. Sabatier. 1996. Chemical synthesis and characterization of maurotoxin, a short scorpion toxin with four disulfide bridges that acts on K^+ channels. *Eur. J. Biochem.* 242:491–498.

Kharrat, R., P. Mansuelle, F. Sampieri, M. Crest, R. Oughideni, J. V. Rietschoten, M. F. Martin-Eauclaire, H. Rochat, and M. E. Ayeb. 1997. Maurotoxin, a four disulfide bridge toxin from *Scorpio maurus* venom: purification, structure and action on potassium channels. *FEBS Lett.* 406:284–290.

Lebrun, B., R. Romi-Lebrun, M. F. Martin-Eauclaire, A. Yasuda, M. Ishiguro, Y. Oyama, O. Pongs, and T. Nakajima. 1997. A four-disulphide-bridged toxin, with high affinity towards voltage-gated K^+ channels, isolated from *Heterometrus spinnifer* (*Scorpionidae*) venom. *Biochem. J.* 328:321–327.

Legros, C., V. Pollmann, H. G. Knaus, A. M. Farrell, H. Darbon, P. E. Bougis, M-F. Martin-Eauclaire, and O. Pongs. 2000. Generating a high affinity scorpion toxin receptor in KcsA-Kv1.3 chimeric potassium channels. *J. Biol. Chem.* 275:16918–16924.

Mackinnon, R., S. L. Cohen, A. Kuo, A. Lee, and B. T. Chait. 1998. Structural conservation in prokaryotic and eukaryotic potassium channels. *Science.* 280:106–109.

Madura, J. D., J. M. Briggs, R. C. Wade, M. E. Davis, B. A. Luty, A. Ilin, J. Antosiewicz, M. K. Gilson, B. Bagheri, L. R. Scott, and J. A. McCammon. 1995. Electrostatic and diffusion of molecules in solution: simulations with the University of Houston Brownian dynamics Program. *Comp. Phys. Commun.* 91:57–95.

Madura, J. D., M. E. Davis, M. K. Gilson, R. C. Wade, B. A. Luty, and J. A. McCammon. 1994. Biological applications of electrostatic calculations and Brownian dynamics simulations. *Rev. Comp. Chem.* 5:229–267.

Matthew, J. B. 1985. Electrostatic effects in proteins. *Annu. Rev. Biophys. Chem.* 14:387–417.

Matthew, J. B., and F. R. Gurd. 1986. Calculation of electrostatic interactions in proteins. *Methods Enzymol.* 130:413–436.

McDonald, I. K., and J. M. Thornton. 1994. Satisfying hydrogen bonding potential in proteins. *J. Mol. Biol.* 238:777–793.

Meiri, N., C. Ghelardini, G. Tesco, N. Galeotti, D. Dahi, D. Tomsic, S. Cavallaro, A. Bartolini, and D. L. Alkon. 1997. Reversible antisense inhibition of *Shaker*-like Kv1.1 potassium channel expression impairs associative memory in mouse and rat. *Proc. Natl. Acad. Sci. U.S.A.* 94:4430–4434.

Miller, C. 1995. The charybdotoxin family of K^+ channel-blocking peptides. *Neuron.* 15:5–10.

Nicholls, A., K. A. Sharp, and B. Honig. 1991. Protein folding and association: insights from the interfacial and thermodynamic properties of hydrocarbons. *Proteins.* 11:281–296.

Northrup, S. H., J. O. Boles, and J. C. L. Reynolds. 1987. Electrostatic effects in the Brownian dynamics of association and orientation of heme protein. *J. Phys. Chem.* 91:5991–5998.

Northrup, S. H., T. Laughner, and G. Stevenson. 1999. MacroDox macromolecular simulation program. Tennessee Technological University, Cookeville, TN.

Northrup, S. H., K. A. Thomasson, C. M. Miller, P. D. Barker, L. D. Eltis, J. G. Guillemette, S. C. Inglis, and A. G. Mauk. 1993. Effects of charged amino acid mutations on the bimolecular kinetics of reduction of yeast iso-1-ferricytochrome c by bovine ferrocytochrome b5. *Biochemistry.* 32:6613–6623.

Olamendi-Portugal, T., F. Gomez-Lagunas, G. B. Gurrola, and L. D. Possani. 1996. A novel structural class of K channel blocking toxin from the scorpion *Pandinus imperator*. *Biochem. J.* 315:977–981.

Ouporov, I. V., H. R. Knull, and K. A. Thomasson. 1999. Brownian dynamics simulations of interactions between aldolase and G- or F-actin. *Biophys. J.* 76:17–27.

Pearson, D. C., and E. L. Gross. 1998. Brownian dynamics study of the interaction between plastocyanin and cytochrome f. *Biophys. J.* 75: 2698–2711.

Smart, S. L., V. Lopantsev, C. L. Zhang, C. A. Robbins, H. Wang, S. Y. Chiu, P. A. Schwartzkroxin, A. Messing, and B. L. Tempel. 1998. Deletion of the Kv1.1 potassium channel causes epilepsy in mice. *Neuron.* 20:809–819.

Smoluchowski, M. V. 1917. Versuch einer mathematischen Theorie der Koagulationskinetik Kolloider Loeschungen. *Z. Phys. Chem.* 92: 129–168.

Thompson, J. D., D. G. Higgins, and T. J. Gibson. 1994. CLUSTAL W: improving the sensitivity of progressive multiple sequence alignment through sequence weighting, position-specific gap penalties and weight matrix choice. *Nucleic Acids Res.* 22:4673–4680.

Wallace, A. C., R. A. Laskowski, and J. M. Thornton. 1995. LIGPLOT: a program to generate schematic diagrams of protein-ligand interactions. *Protein Eng.* 8:127–134.

Warwicker, J., and H. C. Watson. 1982. Calculation of the electric potential in the active site cleft due to alpha-helix dipoles. *J. Mol. Biol.* 157: 671–679.

Zacharias, M., B. A. Luty, M. E. Davis, and J. A. McCammon. 1992. Poisson-Boltzmann analysis of the λ receptor-operator interaction. *Biophys. J.* 63:1280–1285.